

## Magnetic-ion-lattice interaction: Rare-earth antimonides

M. E. Mullen, B. Lüthi\*, and P. S. Wang

*Physics Department, Rutgers University, New Brunswick, New Jersey 08903*

E. Bucher, L. D. Longinotti, and J. P. Maita

*Bell Telephone Laboratories, Murray Hill, New Jersey 07974*

H. R. Ott†

*Laboratorium für Festkörperphysik, Eidgenössische Technische Hochschule, 8049 Zürich, Switzerland*

(Received 4 March 1974)

We have investigated the magnetic, elastic, and thermal properties of the LnSb series. For the compounds which do not undergo a structural or magnetic phase transition (PrSb and TmSb), we measured Schottky specific-heat anomalies, Van Vleck susceptibilities, and anomalies in the elastic constants. All these properties can be interpreted quantitatively as effects due to the crystal-field split levels of the ground-state  $J$  multiplet. For the compounds which undergo magnetic phase transitions (SmSb and GdSb), we find in the case of SmSb similar effects in the paramagnetic region as for PrSb and TmSb, followed by sharp specific-heat and thermal-expansion anomalies at  $T_N = 2.11$ °K. In GdSb we find elastic anomalies for  $T < T_N = 24.4$ °K due to domain-wall stress effects which can be partly removed by application of a magnetic field. DySb, HoSb, and ErSb undergo magnetic and structural transitions at  $T_N = 9.5, 5.25,$  and  $3.53$ °K, respectively. We observe softening of the  $c_{11} - c_{12}$  mode for DySb and HoSb, which can be interpreted quantitatively. In ErSb no elastic mode softens for  $T > T_N$ , indicating that the structural transition involves a coupling of the magnetic ion to other modes than the macroscopic strain. Large thermal-expansion anomalies are observed, especially for ErSb with  $H \sim 6$  kOe, with strong domain-wall stress effects for the elastic modes for  $H \leq 6$  kOe and  $T < T_N$ . A magnetic field cannot separate the structural and magnetic transition temperatures ( $T_a = T_N$ ) but can only cause both to shift to lower temperatures. The magnetoelastic coupling constants, determined from the temperature dependence of the elastic constants, can be interpreted for the LnSb series as being due to the strain modulation of the crystal field.

### I. INTRODUCTION

Recently we showed the effect of crystal-field energy levels on elastic constants for the case of PrSb.<sup>1</sup> We could explain the observed temperature dependence of some symmetry elastic constants using the strain modulation of the crystal field. Here we would like to extend this work by showing this effect for other rare-earth compounds: the rare-earth antimonides (LnSb), where one finds a rich variety of elastic, structural, and magnetic effects. In addition to the temperature dependence of the elastic constants, we give experimental results for their magnetic-field dependence, some specific-heat and susceptibility results, and thermal-expansion measurements.

All these experimental techniques measure thermodynamic equilibrium properties. The effects of crystal-field energy levels on the specific heat (Schottky anomaly) and susceptibility (Van Vleck susceptibility) are well documented for a variety of materials.<sup>2</sup> The specific heat gives a measure of the crystal-field level splittings, the magnetic susceptibility probes the dipole matrix elements if exchange is negligible, and the elastic constants, as strain susceptibilities, probe various electric quadrupole matrix elements. Thermal-expansion

measurements are used here to determine certain aspects of structural transitions.

The rare-earth antimonide series is very well suited for such an investigation: They have the cubic rocksalt structure at room temperature. At low temperatures, some of the compounds undergo magnetic<sup>3</sup> and crystallographic<sup>4</sup> phase transitions. The ground-state multiplet, which is split by the crystal field typically of the order of a few hundred degrees, has been investigated previously with inelastic neutron-scattering techniques for various compounds.<sup>5</sup> Therefore the crystal-field parameters are known. We can use this information for a quantitative analysis of our experimental results.

Our findings are the following: We can quantitatively interpret the temperature dependence of the specific heat, magnetic susceptibility, and elastic constants in the paramagnetic region. The latter measurements give magnetoelastic coupling constants, which vary in a well-determined way across the rare-earth series (depending on the lattice constants and the Stevens  $\alpha$  parameter). From this analysis we can predict which compounds undergo structural instabilities due to this magnetic ion-strain coupling and for which compounds this coupling is too weak to have such an effect. In the low-temperature phase, we observe

TABLE I. Crystal-field parameters for the rare-earth antimonides.

| Compound with electronic ground state | Lattice constant $2a$ (Å) | $A_4\langle r^4 \rangle$ (°K) | $A_6\langle r^6 \rangle$ (°K) | References and remarks |
|---------------------------------------|---------------------------|-------------------------------|-------------------------------|------------------------|
| LaSb ( $4f^0$ )                       | 6.49                      | ...                           | ...                           |                        |
| PrSb ( $4f^2$ ) $^3H_4$               | 6.376                     | 96                            | 2.0                           | 5                      |
| SmSb ( $4f^5$ ) $^6H_{5/2}$           | 6.261                     | 72.5                          |                               | this work              |
| GdSb ( $4f^7$ ) $^8S_{7/2}$           | 6.218                     | ...                           | ...                           |                        |
| DySb ( $4f^9$ ) $^6H_{15/2}$          | 6.160                     | 86                            | 4.2                           | interpolated           |
| HoSb ( $4f^{10}$ ) $^5I_8$            | 6.130                     | 81                            | 4.6                           | interpolated           |
| ErSb ( $4f^{11}$ ) $^4I_{15/2}$       | 6.106                     | 81                            | 4.7                           | 27                     |
| TmSb ( $4f^{12}$ ) $^3H_6$            | 6.084                     | 79.7                          | 5.1                           | 5                      |

strong effects for the elastic constants due to the domains. In cases where one has both a structural and a magnetic phase transition whose transition temperatures coincide, a magnetic field cannot separate them (with the possible exception of HoSb, as discussed below).

In Sec. II, we briefly discuss the theory necessary for the interpretation of our results. In Sec. III we describe our experiment, and in Sec. IV we present and discuss our results.

## II. THEORY

The crystal-field Hamiltonian for  $O_h$  symmetry can be written

$$\mathcal{H}_{CF} = A_4 \langle r^4 \rangle \chi_4 (O_4^0 + 5O_4^4) + A_6 \langle r^6 \rangle \chi_6 (O_6^0 - 21O_6^4), \quad (1)$$

where the  $O_n^m$  are the Stevens operator equivalent and the  $\chi_n$  are reduced matrix elements.<sup>6</sup>  $A_4 \langle r^4 \rangle$  and  $A_6 \langle r^6 \rangle$  can be determined experimentally, for example, from inelastic neutron-scattering experiments and specific-heat measurements. In Table I we have listed these values. They were used to calculate the crystal-field split energy levels of the ground-state manifold.<sup>7</sup>

The Schottky specific heat per ion is

$$C_m = 2kT \frac{\partial}{\partial T} \ln Z + kT^2 \frac{\partial^2}{\partial T^2} \ln Z, \quad (2)$$

where the partition function  $Z \equiv \sum_n e^{-E_n/kT}$ .

Likewise, the Van Vleck susceptibility is given by

$$\chi = kT \frac{\partial^2}{\partial H^2} \ln Z, \quad (3)$$

where  $E(\Gamma_i, H)$  is determined from

$$|E_0(\Gamma_i) - E - \langle \Gamma_i' | g\mu_B H J_z | \Gamma_i \rangle| = 0. \quad (3a)$$

Experimental examples for  $C_m$  and  $\chi$  are given in Figs. 3, 4, and 8 below.

For the symmetry elastic constants  $c_{11} - c_{12}$ ,  $c_{44}$ , and  $c_{11} + 2c_{12}$  we can write a magnetic-ion-lattice interaction<sup>1,8</sup>:

$$\mathcal{H}'(c_{11} - c_{12}) = -g_2 \left( \frac{c_{11}^0 - c_{12}^0}{N} \right)^{1/2} \sum_i (\epsilon_2 O_{2i}^2 + \epsilon_3 O_{2i}^0),$$

$$\mathcal{H}'(c_{44}) = -g_3 \left( \frac{c_{44}^0}{N} \right)^{1/2} \sum_i 2\epsilon_{xy} (J_x J_y + J_y J_x)_i + \dots,$$

$$\mathcal{H}'(c_{11} + 2c_{12}) = -g_1 \left( \frac{c_{11}^0 + 2c_{12}^0}{N} \right)^{1/2} N J^2 (\epsilon_{xx} + \epsilon_{yy} + \epsilon_{zz}). \quad (4)$$

Here the  $c_{ij}^0$  are the background elastic constants,  $\epsilon_2 = 2^{-1/2}(\epsilon_{xx} - \epsilon_{yy})$  and  $\epsilon_3 = 6^{-1/2}(2\epsilon_{zz} - \epsilon_{xx} - \epsilon_{yy})$  are symmetry strains, and  $O_2^2/\sqrt{3} = J_x^2 - J_y^2$  and  $O_2^0 = 2J_x^2 - J_x^2 - J_y^2$  are the Stevens operators acting on the rare-earth ions. The sum is performed over all the rare-earth ions. The  $g_i$  are the magnetoelastic coupling constants. Equation (4) can be obtained by expanding the crystal-field potential in terms of the strains  $\epsilon_{ij}$ . This gives for the coupling constants  $g_2$  and  $g_3$  the following point-charge-calculation expression for the octahedral symmetry:

$$g_2 = \frac{9}{\sqrt{6}} \left( \frac{N}{c_0} \right)^{1/2} \alpha_J \langle r^2 \rangle \frac{Z e^2}{a^3}, \quad (5)$$

$$g_3 = \frac{3}{2} \left( \frac{N}{c_0} \right)^{1/2} \alpha_J \langle r^2 \rangle \frac{Z e^2}{a^3}.$$

Similarly, as for the case of the magnetic susceptibility mentioned above, one can calculate from Eq. (4) the strain dependence of the energy levels<sup>1</sup>:

$$|E_0(\Gamma_i) - E + \langle \Gamma_i' | \mathcal{H}' | \Gamma_i \rangle| = 0. \quad (3b)$$

We solved Eq. (3b) using second-order perturbation theory and obtained the isothermal elastic constants as a strain susceptibility due to the crystal field:

$$c_{ij} = -kT \frac{\partial^2}{\partial \epsilon_i \partial \epsilon_j} \ln Z. \quad (6)$$

Calculations for the elastic constants  $c_{11} - c_{12}$  and  $c_{44}$  based on Eqs. (4) and (6) with the energy-level scheme from Table I are shown in Figs. 1 and 2. The double logarithmic plots show the relative elastic-constant change divided by  $g_i^2$ :  $(c - c_0)/c_0 g_i^2 \equiv f_i(T)$ . One can divide the various materials into two classes: the ones which show characteristic minima or shoulders but remain finite for all temperatures, and the ones which soften as  $T \rightarrow 0$ . In the first class (PrSb, SmSb, DySb, and TmSb), the lowest crystal-field level  $\Gamma_1$  has a vanishing quadrupole matrix element:  $\langle \Gamma_1' | \mathcal{H}' | \Gamma_1 \rangle = 0$ . In these substances  $\Gamma_i$  is  $\Gamma_1$  (for PrSb and TmSb),  $\Gamma_7$  (for SmSb), and  $\Gamma_6$  (for DySb). In the other class,  $\langle \Gamma_i' | \mathcal{H}' | \Gamma_i \rangle \neq 0$  (for HoSb and ErSb). Here  $\Gamma_i$  stands for  $\Gamma_3$  or  $\Gamma_8$ . One expects a structural phase transition, triggered by this magnetic-ion-lattice interaction, to occur in this latter case, whereas in the first case a structural transition should occur only for a large enough  $g_i$ . The condition for a structural instability is

$$c = c_0 + c_0 g_i^2 f_i(T) = 0 \text{ or } g_i^2 f_i(T) = -1. \quad (7)$$

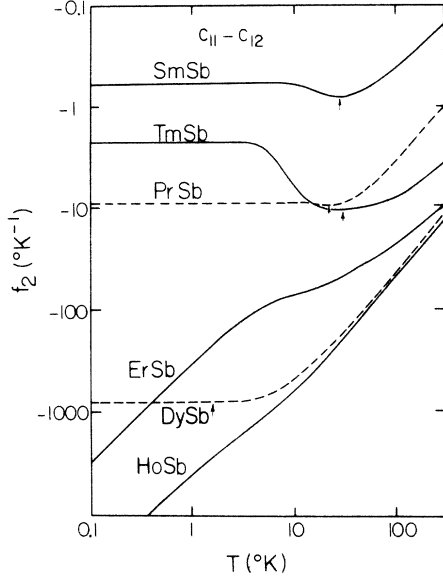


FIG. 1. Temperature dependence of the function  $f_2 \equiv (c - c_0)/c_0 g_2^2$  for the various LnSb. Arrows indicate minima in  $f_2$ .

One important result of our investigation is to give experimental results for the various  $g_i$  and to give an explanation for their systematic variation across the LnSb series.

It is known from other work on the cooperative Jahn-Teller effect<sup>9,10</sup> that in order to describe such a structural transition completely, one often has to include other interactions than the ones given in Eq. (4). The structural instability can be caused by a coupling of the magnetic ion to other modes of the system, e. g., optical phonons, direct interactions, etc. Therefore we generalize Eq. (4) to<sup>9</sup>

$$\begin{aligned} \mathcal{H}' = & -g_2 \left( \frac{c_{11}^0 - c_{12}^0}{N} \right)^{1/2} \sum_i (\epsilon_2 O_{2i}^2 + \epsilon_3 O_{2i}^0) \\ & - g' \left( \frac{A}{N} \right)^{1/2} \sum_i (\langle O_2^0 \rangle O_{2i}^0 + \langle O_2^2 \rangle O_{2i}^2). \quad (8) \end{aligned}$$

Here the other quadrupole-quadrupole interactions have been written down in molecular-field approximation. If we denote the structural transition temperature by  $T_a$ , the elastic constant  $c_{11} - c_{12}$  for  $T > T_a$  is

$$c_{11} - c_{12} = (c_{11}^0 - c_{12}^0) \frac{1 + (g_2^2 + g'^2) f_2(T)}{1 + g_2^2 f_2(T)}, \quad (9)$$

where  $f_2(T)$  is the function defined above and shown in Fig. 1. Equation (9) was first derived by Levy.<sup>11</sup> An elementary derivation is given in the Appendix. Equation (9) and slight modifications and simplifications were successfully used to test mode softening in various materials: TmCd,<sup>12</sup> DySb,<sup>13</sup> DyVO<sub>4</sub>,<sup>14</sup> and NiCr<sub>2</sub>O<sub>4</sub>.<sup>15</sup> Note that for  $T \ll \Delta$ ,  $f(T)$

$\propto -1/T$ , where  $\Delta$  is the gap between the lowest and next higher crystal-field level and where this holds only for the second class of substances discussed above. Depending on the relative magnitude of  $g_2$  and  $g'$ , the elastic constants show strong, medium, or no softening at all as  $T$  approaches  $T_a$ . In Sec. IV we will give experimental results for these various cases.

### III. EXPERIMENT

The LnSb samples used in this investigation were grown by direct fusion and subsequent solidification in a sealed tantalum crucible over a large temperature gradient. This produced crystallites of varying sizes, depending on the particular rare-earth compounds. Single crystals were cut out with a spark cutter and oriented using an x-ray goniometer. In most cases at least two crystals were investigated.

Starting materials were Sb (United Mineral and Chemical Corp.) with a 99.999% purity; the various rare earths typically were of 99.9% purity and were obtained from Rare Earth Products (La, Sm, and Gd), U. S. Bureau of Mines (Pr), Lunex (Dy, Ho, and Er), and Research Chemicals (Tm). With the exception of the Lunex materials, all rare earths contained between 0.1 and 0.5% gas impurities, which may account for some variations in physical properties, such as  $T_N$ .

Susceptibility measurements were made with a pendulum magnetometer.<sup>16</sup> Specific-heat experiments were performed in a heat-pulse calorimeter

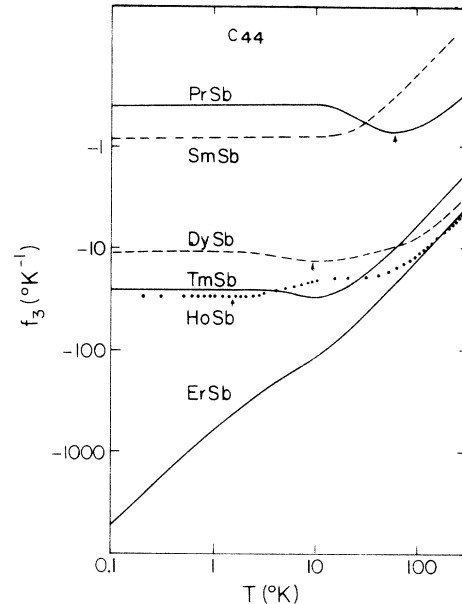


FIG. 2. Temperature dependence of the function  $f_3 \equiv (c - c_0)/c_0 g_3^2$  for the various LnSb. Arrows indicate minima in  $f_3$ .

described elsewhere.<sup>17</sup>

The elastic constants were measured with a phase-comparison method,<sup>18</sup> in most cases capable of detecting velocity changes in these substances of one part in  $10^6$ . In all cases, no thermal-expansion corrections were necessary, the fractional-velocity changes being always much larger than the fractional-length changes. The measuring frequency was either 10 or 30 MHz.

For the thermal-expansion measurements we used a capacitance dilatometer. The samples, with linear dimensions on the order of 2–3 mm, and the sample holder were initially cooled to 1.5 °K. By raising the temperature in small steps of approximately 0.03–0.05 °K, we then determined the length changes due to the thermal expansion of the crystals relative to copper. In this temperature region, the thermal expansion of copper is several orders of magnitude smaller than that of the substances investigated, and any corrections due to expansion of the capacity cell can be neglected.

As thermometers we used thermocouples, Germanium resistors (CryoCal), capacitance thermometers (Lake Shore Cryotronics), and a helium vapor-pressure manometer, depending on the temperature region and on the presence of magnetic fields. The magnetic field was generated either by electromagnets or by high-field superconducting magnets.

#### IV. RESULTS AND DISCUSSION

We organize this section in the following way: First, we discuss the materials which exhibit neither a magnetic nor a structural transition at any finite temperature (LaSb, PrSb, and TmSb). Second, we discuss samples which exhibit only a magnetic phase transition (SmSb and GdSb). Then we treat the cases where both a magnetic and a structural transition occur (DySb, HoSb, and ErSb). Finally, we compare and interpret some physical quantities for the whole LnSb series (elastic constants and magnetoelastic coupling constants). A short account of this work was given elsewhere.<sup>19</sup>

##### A. Case of no phase transitions (LaSb, PrSb, and TmSb)

In these compounds we did not find any evidence for a magnetic or structural transition down to ~1 °K. In both PrSb and TmSb, the lowest crystal field state is a  $\Gamma_1$ .

In Fig. 3 we show the magnetic specific heat for TmSb. The lattice and electronic specific heat was subtracted using specific-heat measurements for LuSb. The result in Fig. 3 exhibits a marked Schottky anomaly with a maximum at ~11 °K. The full line is the calculated one, using the crystal-field parameters listed in Table I and Eq. (2). The

agreement between experiment and calculation is quite satisfactory.

As an example of the Van Vleck susceptibility, we show data for PrSb in Fig. 4. These results show the expected behavior, a linear temperature dependence at high temperatures for  $\chi^{-1}$  and a successively weaker temperature dependence towards lower temperatures. Again the full curve shows the calculated susceptibility, using the crystal-field parameters listed in Table I and Eq. (3). The agreement with the experiment is again quite satisfactory. From the high-temperature slope at about 300 °K, we get an experimental effective Bohr-magneton number  $p = g\{[J(J+1)]^{1/2}\} = 3.61$  compared to the free-ion value of 3.58. It should be noted that in this interpretation of the susceptibility, exchange effects were neglected.

Turning now to the elastic constants, we show in Fig. 5 the temperature dependence of the  $c_{44}$  and the  $c_{11}-c_{12}$  modes for LaSb. Absolute values for the LnSb series at 200 °K, together with densities and Debye temperatures, are given in Table II. The LaSb data exhibit normal behavior—a stiffening with lower temperatures and a temperature independence at the lowest temperatures. We use the LaSb data as a background estimate for the other samples.

In contrast to this, the elastic constants of PrSb and TmSb show a more complicated temperature dependence. In Fig. 6 we see that for PrSb, all the modes exhibit characteristic minima of a few percent of the elastic constant ( $c_{11} - c_{12}$ ) at 23 °K and

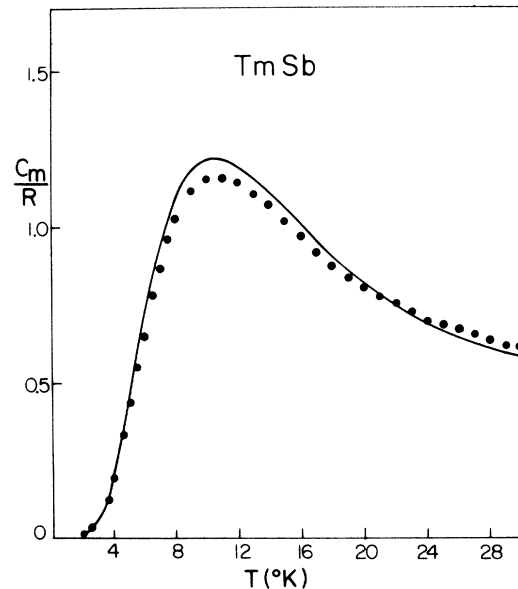


FIG. 3. Schottky specific heat for TmSb, with lattice and electronic specific heat subtracted. Full circles are experimental points, full line is calculated curve with parameters listed in Table I.

TABLE II. Physical constants determined from our experiments.

| $T_N$<br>(°K) | Density $\rho_x$<br>(g/cm <sup>3</sup> ) | Elastic<br>constants (200 °K)                       |                   | Debye<br>temperatures $\theta$<br>(°K) | Magnetoelastic<br>coupling constants (m°K) |                 |                              |
|---------------|--|---|-------------------|--|--|-----------------|------------------------------|
|               |  | $c_{44}$<br>(10 <sup>11</sup> dyn/cm <sup>2</sup> ) | $c_{11} - c_{12}$ |  | $g_3^2$ (expt.)                            | $g_2^2$ (expt.) | $g_2^2$ (calc.) <sup>a</sup> |
| LaSb          | 6.33                                     | 1.95  | 7.4               | 211 (225)                              |  |                 |                              |
| PrSb          | 6.77                                     | 2.00  | 11.0              | 221                                    | 5.4  | 4.9             | 168                          |
| SmSb          | 2.11                                     | 7.37  | 2.27              | 232                                    | 14   | 38              | 431                          |
| GdSb          | 24.4                                     | 7.70  | 2.37              | 233                                    |  |                 |                              |
| DySb          | 9.5                                      | 8.10  | 2.60              | 241                                    |  | 1.3             | 7                            |
| HoSb          | 5.25                                     | 8.27  | 2.76              | 247                                    | 1.1  | 0.11            | 0.75                         |
| ErSb          | 3.53                                     | 8.42  | 2.60              | 237                                    |  | <0.2            | 1.1                          |
| TmSb          | 8.57                                     | 2.68  | 13.5              | 237                                    | 1.4  | 1.2             | 17                           |

<sup>a</sup> $g_2^2$ (calc.) was obtained from Eq. (5) with  $Z = -2$ ,  $\langle \rho^2 \rangle$  from A. J. Freeman and R. E. Watson, Phys. Rev. **127**, 2058 (1962) and neglecting shielding factors.

$c_{11}$  at 25 °K and the longitudinal [110] mode ( $c_{11} + c_{12} + 2c_{44}$ ) at 28 °K. Below the minima, the elastic constant no longer reaches its value of the high-temperature side, and becomes independent below 8 °K. These features were already shown and explained before<sup>1</sup> using Eqs. (4) and (6), i.e., the calculated functions  $f_i(T)$  shown in Figs. 1 and 2. Here we give a more complete comparison between experiment and theory for all the modes shown in Fig. 6. We first fitted the symmetry modes  $c_{11} - c_{12}$  and  $c_{44}$  using the LaSb data for the background temperature dependence. In such a procedure one fixes two points of the curve, determining the coupling constant  $g_i$  and the absolute value of the background elastic constant  $c_0$ . One notices a good fit

to the experimental data for the  $c_{11} - c_{12}$  mode and a lesser degree of agreement for the  $c_{44}$  mode, as noted before.<sup>1</sup> However, since the  $c_{44}$  mode has a much smaller absolute value than the other elastic constants, it does not seriously affect their fit. The composite elastic constants  $c_{11}$  and  $c_{11} + c_{12} + 2c_{44}$  can be expressed as linear combinations of the three symmetry elastic constants, with the bulk modulus  $c_{11} + 2c_{12}$  having no temperature dependence in the approximation of Eq. (4). Also, these composite elastic constants can be interpreted satisfactorily, the salient features of the experimental data being well reproduced by our calculation. The magnetoelastic coupling constants  $g_2$  and  $g_3$ , determined from the fit in Fig. 6, are listed in Table II.

Similar behavior of the temperature dependence of the elastic constants for TmSb can be seen in Fig. 7. Again the calculations, as taken from

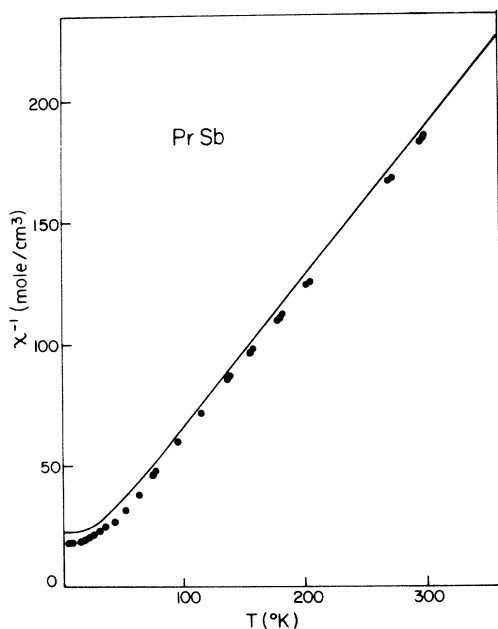


FIG. 4. Inverse magnetic susceptibility for PrSb. Full circles are experimental points, full line is calculated susceptibility with parameters listed in Table I, exchange neglected.

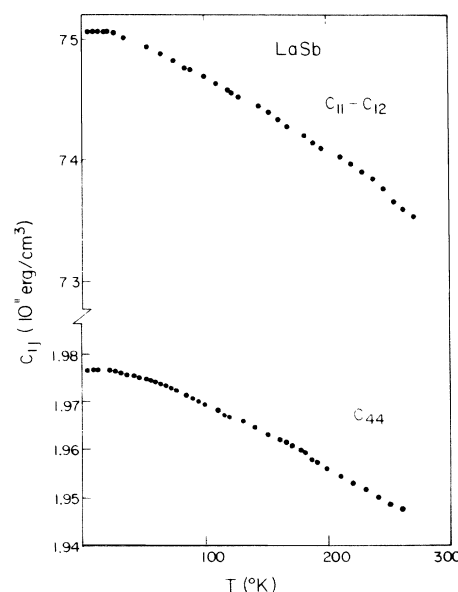


FIG. 5. Temperature dependence of the elastic constants  $c_{44}$  and  $c_{11} - c_{12}$  for LaSb.

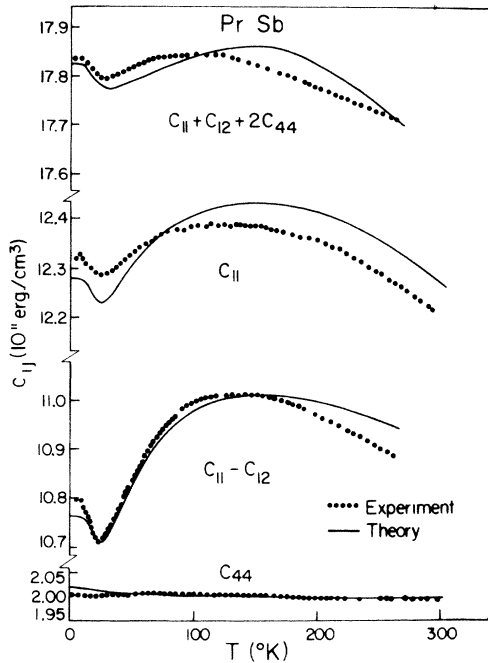


FIG. 6. Temperature dependence of various elastic constants for PrSb. Full circles are experimental points, full lines are from calculations explained in the text.

Figs. 1 and 2, fit the measured curves very nicely, especially the  $c_{44}$  mode and, to a lesser extent, the  $c_{11}-c_{12}$  mode. The coupling constants, determined from this fit, are also listed in Table II.

For the interpretation of the thermodynamic quantities  $C_m$ ,  $\chi$ , and  $c_{ij}$  for the two substances PrSb and TmSb, we neglected the effects of exchange and quadrupole-quadrupole interactions

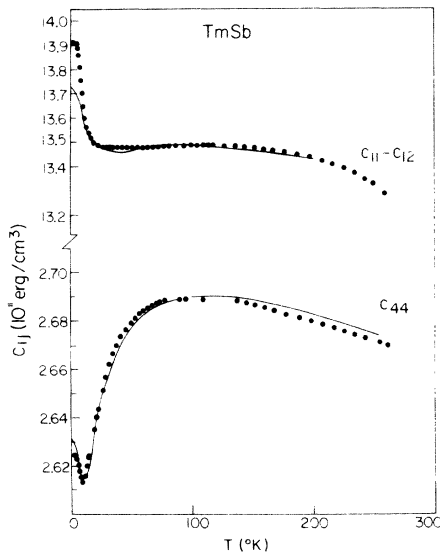


FIG. 7. Temperature dependence of the symmetry elastic constants for TmSb. Full circles are from experiment, full lines are calculated curves.

completely; that is, we used Eqs. (3) and (3a) and Eq. (9) with  $g'=0$ . The generally good agreement between experiment and theory, together with the absence of any magnetic and structural phase transition, seems to justify this procedure. Inclusion of  $g'$  does not change the temperature of the minima for the elastic constants.

In TmSb, we observed at  $2^\circ\text{K}$  a very small anomaly in the specific heat, electrical resistivity, and elastic constants. This anomaly, the origin of which we do not know, is so small that it is not discernible in Figs. 3 and 7.

Application of a magnetic field has a very small effect on the elastic constants. As an example in PrSb, the  $c_{11}$  mode with a 50-kOe field applied in the [100] direction experiences a fractional velocity change of  $2 \times 10^{-4}$  at  $26^\circ\text{K}$  and of  $8 \times 10^{-4}$  at  $12^\circ\text{K}$ .

Finally, with the magnetoelastic coupling constants listed in Table II, one can ask: How much larger must these  $g_i$  be in order to induce a structural transition? The answer is, using Eq. (7), about 20 times larger for PrSb and 25 times larger for TmSb. The reason for this is the rather small value for the function  $f_i$  in Figs. 1 and 2, because in this case there are no quadrupole matrix elements between the ground state  $\Gamma_1$  and the next higher  $\Gamma_4$ . In PrSb, the first nonvanishing matrix element out of the ground state is  $\Gamma_1-\Gamma_3$  ( $125^\circ\text{K}$ ), which affects  $c_{11}-c_{12}$ , and in TmSb it is  $\Gamma_1-\Gamma_5$  ( $56^\circ\text{K}$ ), which affects  $c_{44}$ .

#### B. Case of magnetic phase transition (SmSb and GdSb)

SmSb has a  $\Gamma_7$  ground state. In Fig. 8 we show the specific heat for SmSb as a function of temperature. The lattice specific heat was subtracted, using a weighted average of the LaSb and LuSb specific heat. It exhibits a clear Schottky anomaly

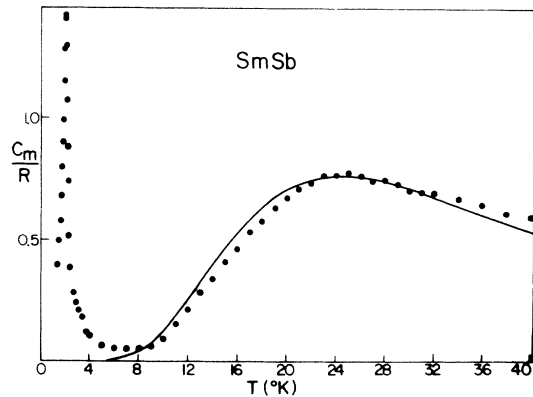


FIG. 8. Temperature dependence of the specific heat for SmSb with lattice specific heat subtracted. Full circles are experimental points, full line is fit to Schottky anomaly with parameters taken from Table I.

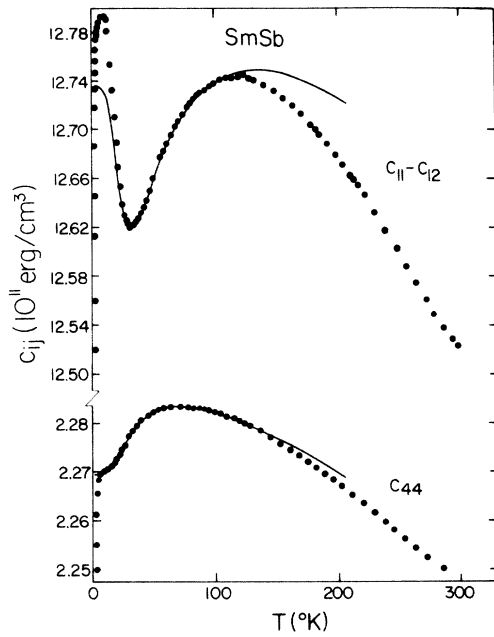


FIG. 9. Temperature dependence of symmetry elastic constants for SmSb. Full circles are experimental points, full line is theoretical fit for the crystal-field effects.

near 25 °K and a sharp anomaly at the magnetic phase transition  $T_N = 2.11$  °K. The full line gives the best fit to the crystal-field anomaly. The cor-

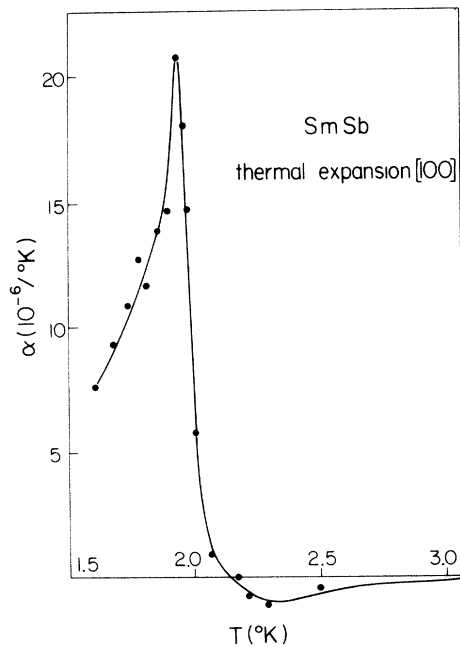


FIG. 10. Temperature dependence of thermal expansion for SmSb. Full circles are experimental points, full line is guide to eye.

responding  $A_4$  parameter listed in Table I gives a  $\Gamma_7$  ground state and a  $\Gamma_7$ - $\Gamma_8$  separation of  $65 \pm 3$  °K. To our knowledge, this is the first determination of  $T_N$  and  $A_4 \langle r^4 \rangle$  for SmSb.

The symmetry elastic constants for SmSb are shown in Fig. 9. The  $c_{11}-c_{12}$  mode exhibits a minimum at 30 °K of about 1%, while  $c_{44}$  has only a shoulder at about 14 °K. Both elastic constants begin to soften below 4 °K and show strong softening in the ordered region. At  $T_N$  there is a kink in the elastic-mode curve, which, while not discernible in Fig. 9, can be seen in Fig. 11(a). The features due to the crystal field in these elastic constants are well reproduced by our calculation (solid line in Fig. 9). The magnetoelastic coupling constants deduced from this fit are listed in Table II. Using Eq. (7), we conclude that  $g_2^2$  is 31 times too small to induce a structural transition based on the mechanism of Eq. (4). While other coupling mechanisms, such as the one discussed in Eq. (8), cannot be excluded, additional information, such as the thermal-expansion measurements shown in Fig. 10, strongly suggests that the transition at  $T_N$  is purely magnetic. The measured thermal-expansion anomaly of  $\alpha \sim 20 \times 10^{-6}$  is of the same order of magnitude as that of a representative antiferromagnet,  $\text{MnF}_2$ .<sup>20</sup> Furthermore, a 15-kOe magnetic field does not change the data in Fig. 10. The data in this figure were taken using a different sample

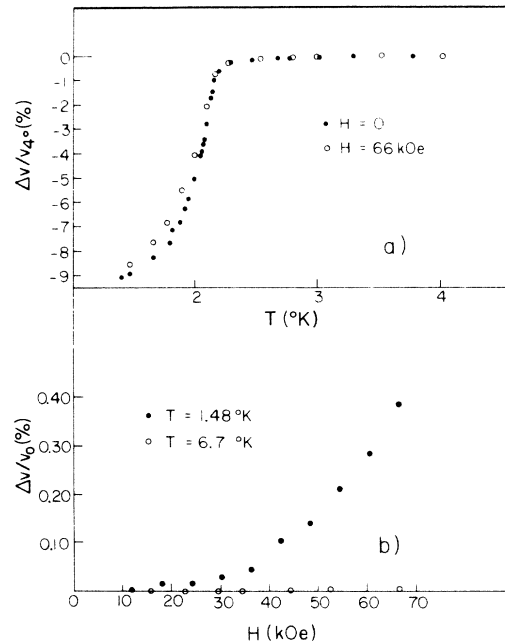


FIG. 11. Temperature and field dependence of  $c_{11}-c_{12}$  mode for SmSb. Plotted are fractional velocity changes; the field is along the [110] axis. (a) Isochamps for  $H = 0$  and 66 kOe, (b) isotherms for two different temperatures.

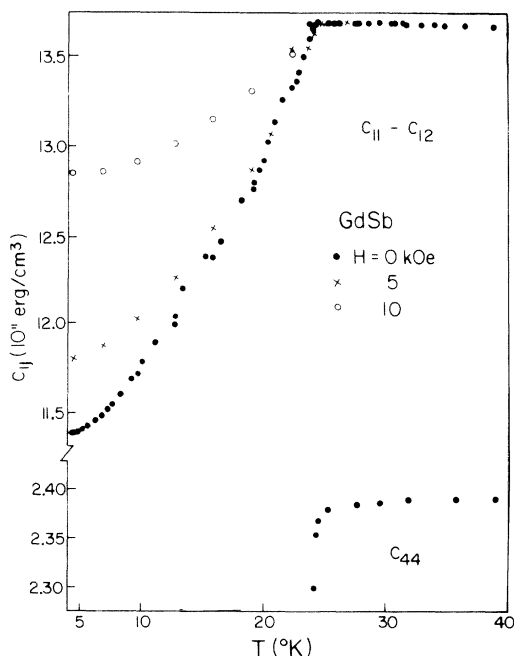


FIG. 12. Temperature and magnetic-field dependence of the  $c_{44}$  and  $c_{11} - c_{12}$  elastic constants for GdSb. Field is along [001] axis. Full circles are  $H = 0$  kOe, crosses are  $H = 5$  kOe, open circles are  $H = 10$  kOe.

than that used for the elastic constants and specific heat, as indicated in the somewhat lower  $T_N \sim 1.95$  °K.

To the best of our knowledge, nothing is known so far about the spin order and anisotropy in SmSb. Therefore we cannot discuss quantitatively our magnetoelastic measurements shown in Fig. 11. The velocity change in an applied [110] magnetic field is generally very small, about 0.4% at 66 kOe and  $T = 1.5$  °K, and 0.003% at 66 kOe and  $T = 6.7$  °K [Fig. 11(b)]. Furthermore, isochoamps at 66 kOe, together with the zero-field result of Fig. 9, are shown in Fig. 11(a), again demonstrating a rather small magnetic-field effect. This is in agreement with the thermal-expansion results quoted above and quite different from the effects we observe in other crystals (GdSb, DySb, and ErSb) discussed below.

**GdSb.** GdSb has no orbital moment but a spin  $S = \frac{7}{2}$ . No structural distortion at  $T_N$  has been observed,<sup>4</sup> which was expected. In Fig. 12 we show the temperature dependence of the  $c_{11} - c_{12}$  and  $c_{44}$  modes. As expected, the temperature dependence is normal in the paramagnetic region, with no sign of crystal-field effects. Below  $T_N = 24.4$  °K, the elastic constants drop drastically, a change of 15% for the  $c_{11} - c_{12}$  mode down to 4 °K and a change of 4% for the  $c_{44}$  mode at  $T_N$ , where we lost the echo due to strong attenuation. It should be stressed

that the results of Fig. 12 are not very well suited for an accurate determination of  $T_N$ . A recent value<sup>21</sup> for a single crystal gives  $T_N = 24.77$  °K, very close to our estimated value from Fig. 12. Because of the absence of any crystal-field effects in GdSb, no magnetoelastic coupling constants can be obtained with the method described in this paper, and recourse to other techniques must be taken.

Application of a magnetic field has practically no effect on the  $c_{44}$  mode, since it is for  $T > T_N$ . However, a [100] field has a drastic effect on  $c_{11} - c_{12}$  for  $T < T_N$ , as shown in Fig. 12 for 5 and 10 kOe as a function of temperature. A decrease in the velocity anomaly with increasing field is observed in the ordered region. This is similar to elastic-modulus changes observed in various magnetic substances<sup>22</sup> and is probably also due to domain-wall stress effects. Similar effects were observed for the longitudinal [110] mode ( $c_{11} + c_{12} + 2c_{44}$ ). No critical effects, both for velocity and attenuation (10 MHz), were observed at  $T_N$  for this longitudinal mode, but only for  $c_{44}$ . This could imply that  $g_3$  is much larger than  $g_2$  and the volume magnetostrictive coupling constant.<sup>23</sup>

### C. Case of magnetic and structural transition (DySb, HoSb, and ErSb)

In these cases, one finds a structural and magnetic phase transition at the same temperature. We discuss individually the three compounds.

**DySb.** The crystal-field energy levels of this compound have not been measured directly, but an interpolation of the crystal-field parameters of PrSb and TmSb<sup>24</sup> gives the ones listed in Table I

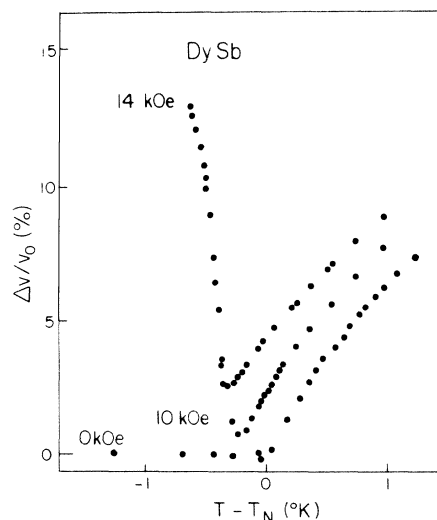


FIG. 13. Magnetoelastic effects in DySb for  $c_{11} - c_{12}$  mode. Given is fractional velocity change in the vicinity of  $T_N$ . Field is along [001] axis.

and a  $\Gamma_6$  ground-state level, followed by a  $\Gamma_8$  level 14.5 °K higher. Previous experiments<sup>4,24</sup> gave a strong tetragonal and a small rhombohedral distortion of first-order nature at  $T_N = 9.5$  °K.

Elastic-constant measurements<sup>13,25</sup> showed a strong softening of the  $c_{11}-c_{12}$  mode and only 0.8% change for the  $c_{44}$  mode at  $T_N$ . The temperature dependence of the  $c_{11}-c_{12}$  mode has been analyzed by Levy<sup>11,13</sup> for  $T > T_N$ . The magnetoelastic coupling constants are listed in Table II. For  $T < T_N$ , a very small temperature dependence is observed,<sup>13</sup> as shown in Fig. 13. This is in disagreement with a recent calculation<sup>26</sup> which predicts an increase in the elastic constant for  $T < T_N$ , as in the case of the Vanadates,<sup>14</sup> except that  $c_{11}-c_{12}$  should show a discontinuity at  $T = T_N$  because of the first-order nature of the transition. In Fig. 13 we show the magnetic-field and temperature dependence for the  $c_{11}-c_{12}$  mode. We found a very strong dependence on the magnetic-field direction; Fig. 13 shows results for a [100] field. One notices for  $T \leq T_N$  a very large increase in velocity for  $H = 14$  kOe. For  $T < T_N - 1$  °K, we lose the echo due to strong attenuation. At least part of this behavior in the elastic constant for  $T < T_N$  can again be ascribed to domain-wall stress effects. These effects were neglected in the theories and interpretations mentioned above<sup>13,26</sup> for  $H = 0$ . Our results show that if one suppresses this effect with a magnetic field, the agreement with theory<sup>26</sup> is improved. No attempt was made here to calculate the elastic constant in a magnetic field due to Zeeman splittings of the energy levels.

*HoSb.* An interpolation procedure between PrSb

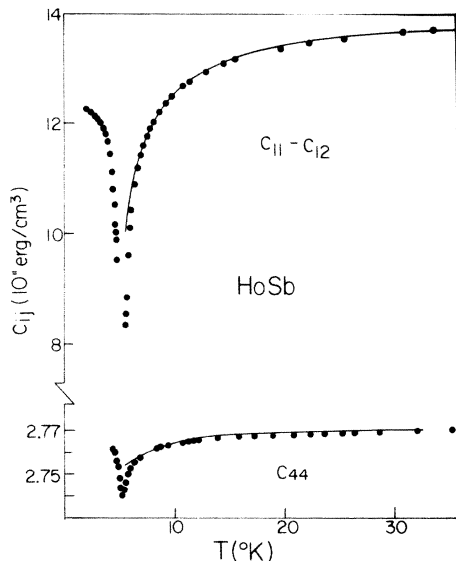


FIG. 14. Temperature dependence of the  $c_{11}-c_{12}$  and  $c_{44}$  modes in HoSb. Full circles are experimental points, full lines are calculated curves.

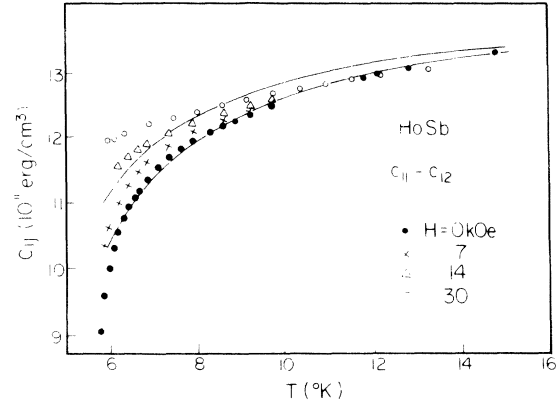


FIG. 15. Temperature and magnetic-field dependence of the elastic symmetry mode  $c_{11}-c_{12}$  for HoSb. Field direction is [110]. Full circles are  $H = 0$  kOe, crosses are  $H = 7$  kOe, triangles are  $H = 14$  kOe, open circles are  $H = 30$  kOe, full lines are calculated curves for  $H = 0$  and 30 kOe.

and TmSb again gives the crystal-field parameters shown in Table I. This leads to  $\Gamma_3$  and  $\Gamma_4$  levels lying very close together. Structural<sup>4</sup> and electrical resistivity data<sup>21</sup> indicate that at  $T_N$  this compound undergoes a cubic to tetragonal lattice distortion presumably of second order.

From Fig. 1 we expect strong softening for the  $c_{11}-c_{12}$  mode. Indeed, as shown in Fig. 14, this mode shows a 40% softening down to 5.6 °K, where we lose the echo due to strong attenuation. In comparison, the  $c_{44}$  mode shows a dip of about 2% from high temperatures down to  $T_N = 5.25$  °K. This value for  $T_N$  is close to a recently determined one of 5.4 °K.<sup>21</sup> The solid curves in Fig. 14 represent the calculated temperature dependence of the elastic constants, using the functions  $f_2$  and  $f_3$  of Figs. 1 and 2, Eq. (9) for  $c_{11}-c_{12}$ , and Eq. (6) for  $c_{44}$ . The agreement with experiment is excellent except when very close to  $T_N$ . The parameters  $g_2$  and  $g_3$  are given in Table II, and  $g'^2 = 0.60$  m °K. With these parameters we get a calculated structural transition at  $T = 4.5$  °K, compared to the experimentally observed one at 5.25 °K. Since the transition is probably very close to second order,<sup>4,21</sup> it is believed that strong critical effects close to  $T_N$ , not taken into account in our analysis and fit, can account for this discrepancy. At  $T = 0$ ,  $g_2$  for HoSb gives a spontaneous strain  $\epsilon_3 \sim 1.3 \times 10^{-3}$ , in fair agreement with a measured one of  $2.4 \times 10^{-3}$ .

Application of magnetic fields along the [110] direction diminished the softening of the  $c_{11}-c_{12}$  mode considerably for  $T > T_N$ , as shown in Fig. 15 for fields up to 30 kOe. Up to 14 kOe, the anisotropy due to field direction is very small. As in the zero-field case, we invariably lost the echoes at  $T \sim T_N$  even in the highest field and were not able to measure below  $T_N$  for this mode. A semiquantita-

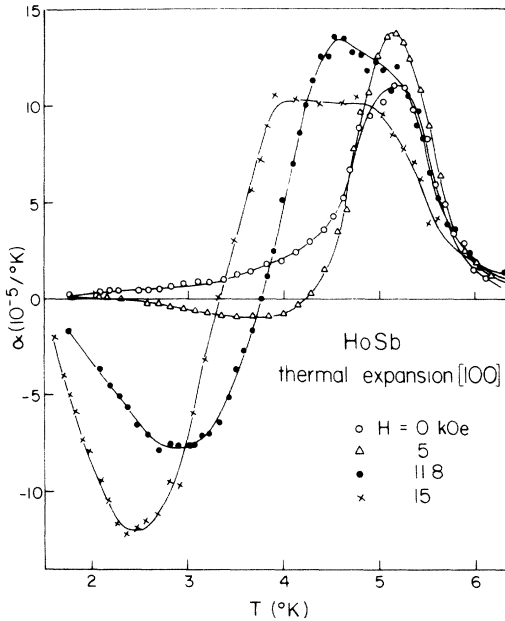


FIG. 16. Thermal expansion in HoSb. Full lines are guide to eye.

tive explanation of the results shown in Fig. 15 lies in the effect of Zeeman split crystal-field levels on the elastic constant. The solid lines in Fig. 14 give the result of such a calculation for  $H = 30$  kOe together with the zero-field result already shown in Fig. 14. For this calculation, we only considered the three lowest crystal-field levels  $\Gamma_3$ ,  $\Gamma_4$ , and  $\Gamma_1$ , neglecting the rest of the  $J = 8$  multiplet with energies of  $80^\circ\text{K}$  and higher. While the agreement with the experimental curve is not perfect, the salient feature is shown: an increase of  $c_{11}-c_{12}$  with field which is more pronounced as one nears  $T_N$ .

(Additional studies with a new sample of HoSb allowed us to measure  $c_{11}-c_{12}$  in the ordered region. These results are included in Fig. 14. They exhibit a temperature dependence as expected from theory,<sup>26</sup> with domain-wall stress effects playing a less important role than in GdSb, DySb, and ErSb.)

Thermal-expansion results for HoSb are shown in Fig. 16 for various magnetic-field strengths. There are several interesting features: Compared to SmSb (Fig. 10) and ErSb (Fig. 19) discussed below, the thermal-expansion results of HoSb exhibit rather broad anomalies. This can be due to strain broadening; our HoSb cleaved very easily. For  $H \neq 0$  there is a sign change in  $\alpha$  at lower temperatures. All these properties are probably responsible for the inability to propagate the  $c_{11}-c_{12}$  mode below  $T_N$ . The thermal-expansion curves for  $H = 11.8$  and  $15$  kOe appear to have two broadened

peaks, as seen in Fig. 16. These features were observed for three different crystals. They could mean, for example, that in a magnetic field the structural and magnetic transition temperatures separate, or that there are additional magnetic or structural transitions for  $H \neq 0$  and  $T < T_N$ , or that there exist pronounced domain effects in this sample. Preliminary  $c_{44}$  measurements for  $T < T_N$  and  $H \neq 0$ , however, do not give clear evidence for a separation of  $T_a$  and  $T_N$ .

**ErSb.** Again the crystal-field parameters shown in Table I are obtained from the same interpolation procedure. The resulting energy splitting seems to explain the observed Schottky anomaly in the specific heat.<sup>27</sup> Nothing is known so far about a structural transition at  $T_N = 3.53^\circ\text{K}$ , except that it is of first order.<sup>27</sup>

From Figs. 1 and 2 we expect strong softening of both the  $c_{11}-c_{12}$  and the  $c_{44}$  mode. Contrary to this, we find an almost temperature-independent variation of all modes in the temperature region  $T > T_N = 3.5^\circ\text{K}$  (Fig. 17), up to more than  $100^\circ\text{K}$ . Below  $T_N$  we observe almost steplike discontinuities in the elastic modes of 2.5% for  $c_{44}$ , 41% for  $c_{11}-c_{12}$ , and 14.5% for  $c_{11}$ . From the behavior for  $T > T_N$ , it apparently follows that  $g' \gg g_i$ . In analogy to the case of SrTiO<sub>3</sub>,<sup>28</sup> we suggested that  $g'$  could, for example, indicate the coupling of the magnetic ion to a zone-boundary phonon.<sup>19</sup> A similar suggestion has recently been made for the case of HoP on theoretical grounds.<sup>29</sup> One has to await neutron-scattering results in order to get more information on this problem. For  $T \sim 200^\circ\text{K}$ , we found a small kink in some elastic constants and in the susceptibility, the origin of which is not known to us. Since for estimating the temperature dependence of the elastic constants we cannot use

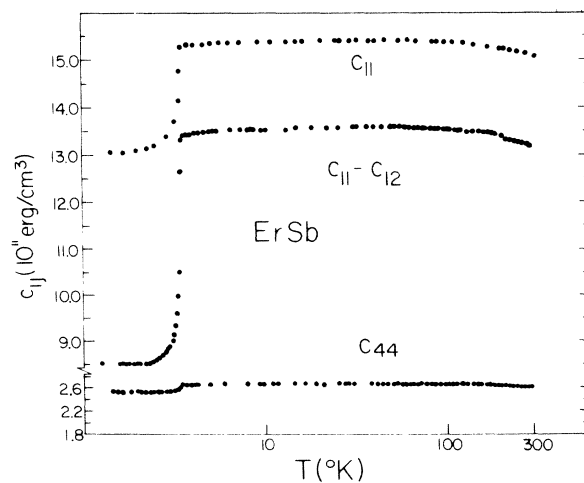


FIG. 17. Temperature dependence of various elastic modes for ErSb. Note logarithmic temperature scale.

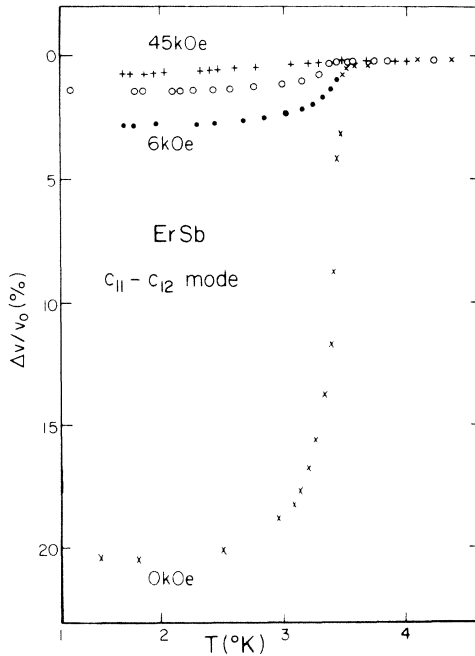


FIG. 18. Magnetoelastic effects in ErSb for  $c_{11} - c_{12}$  mode. Field direction is [110]. Crosses are  $H = 0$  kOe, full circles are  $H = 6$  kOe, open circles are  $H = 18$  kOe, pluses are  $H = 45$  kOe. Given is fractional velocity change.

the functions  $f_i$ , we can give only upper limits for the magnetoelastic coupling constants  $g_i$  in Table II.

Below  $T_N$ , the decrease of the elastic constants is much more rapid than in the case of GdSb (Fig. 12). However, application of a magnetic field has a similar effect as for GdSb, as a comparison of Figs. 12 and 18 shows. In both cases, the anomaly is reduced with increasing magnetic field. In ErSb, a [110] magnetic field of 18 kOe reduces the  $c_{11} - c_{12}$  anomaly from 46 to 1%, with similar results for the  $c_{44}$  mode. A 45-kOe field reduces the anomaly almost completely. Again, as in the case of GdSb, we attribute this effect at least partly to the sound-wave-domain-wall coupling,<sup>22</sup> where in the case of ErSb we deal both with magnetic and structural domains. From a comparison of Figs. 18 and 19, we conclude that the large suppression of the domain-wall stress effect is operative up to about 6 kOe, where it seems that we have a single domain state. The further changes of the elastic constant for higher fields are then truly single-domain magnetoelastic effects. Also discernible from Fig. 18 is a shift of  $T_N$  towards lower temperatures with increasing  $H$ , an effect we observed both in the magnetic susceptibility and thermal expansion as well, as discussed below.

Thermal-expansion measurements for ErSb are shown in Fig. 19. At zero field, one observes an

anomaly at  $T_N = 3.53$  °K which is about an order of magnitude larger than in SmSb. Application of a moderate field of 6.5 kOe increases the anomaly to  $\alpha \sim 75 \times 10^{-5}$  °K<sup>-1</sup>, a very large effect.<sup>30</sup> It is this large  $\alpha$  which leads us to assume that we deal here with a magnetic and a structural transition. It is the alignment of the domains which enhances the effect in a magnetic field. The shift of  $T_N$  with field agrees qualitatively with the elastic results (Fig. 18) and with magnetic-susceptibility results not shown here.

It is of great interest to note that the zero-field as well as the nonzero-field results exhibit only one anomaly as a function of temperature (Fig. 19). Although there exist theoretical models which exhibit successive transitions,<sup>31</sup> the rare-earth pnictides seem to exhibit only one transition, with the magnetic (dipolar) and the structural (quadrupolar) transition coinciding. This was shown before with specific-heat measurements in DySb<sup>24</sup> and in ErSb, ErAs, and ErBi.<sup>27</sup> The fact that a magnetic field cannot separate the magnetic and structural transition (Fig. 19) indicates that this is not a mere coincidence. As discussed above, there is a slight possibility that for HoSb, a magnetic field actually can separate the structural and magnetic transition. However, the experimental evidence (Fig. 16) is not clearcut.

#### D. Comparative elastic and magnetoelastic properties of LnSb

Finally, we would like to discuss common comparative features of the LnSb series, such as elas-

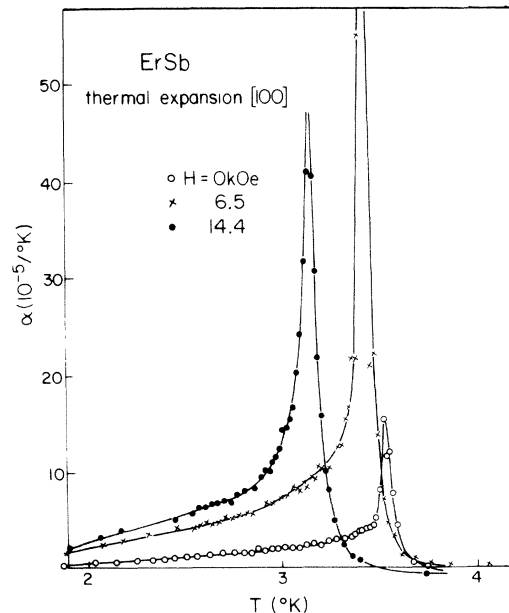


FIG. 19. Thermal expansion in ErSb. Open circles are  $H = 0$  kOe, crosses are  $H = 5.6$  kOe, full circles are  $H = 14.4$  kOe, full lines are guide to eye.

tic constants, Debye temperatures, and magnetoelastic coupling constants determined from our experiment.

*Elastic constants.* In Table II we have listed the absolute elastic constants  $c_{44}$  and  $c_{11}-c_{12}$  for the various rare-earth antimonides. One notices a regular variation of these constants across the series. We shall try to analyze these results in the same way as has been done for the alkali halides.<sup>32</sup> The alkali halides have the same rocksalt structure as the antimonides; the only difference is that the latter are metallic. In the case of the halides, a Born model, based on electrostatic and core-repulsion energies,<sup>32</sup> gave a good account of the situation. Taking the same formulas, we get the following value for these contributions for  $c_{44}$ :  $0.73 \times 10^{11}$  ergs/cm<sup>3</sup> (LaSb) -  $0.94 \times 10^{11}$  ergs/cm<sup>3</sup> (TmSb), i.e., rather little variation across the series and only about  $\frac{1}{3}$  of the elastic constant accounted for with this mechanism. For  $c_{11}-c_{12}$  we get the following with  $\delta=10$ :  $2.7 \times 10^{11}$  ergs/cm<sup>3</sup> (LaSb) -  $3.5 \times 10^{11}$  ergs/cm<sup>3</sup> (TmSb), accounting again for about  $\frac{1}{3}$  of the measured elastic constant. The rest, or  $\frac{2}{3}$ , of the elastic constants obviously must be explained by band-structure effects.<sup>33</sup> Since little is known so far about the electronic band structure of these materials, we have to postpone a further discussion of this point; but it is clear that the series offers a very good test for any such calculation, since the lattice constant is the only important variable for the band structure in LnSb.

*Debye temperatures.* Also listed in Table II are the Debye temperatures for the LnSb compounds, determined<sup>34</sup> from the elastic constants  $\theta_{e1}$  and in some instances from specific-heat measurements (LaSb). Because of the rather small value of the  $c_{44}$  constants,  $\theta_{e1}$  is mainly determined by  $c_{44}$ . One notices a change of about 10% of the Debye  $\theta$  across the series,  $\theta$  being typically 220 °K.

*Magnetoelastic coupling constants.* The magnetic-ion-strain-coupling constants  $g_2$  and  $g_3$  also are listed in Table II. They were obtained from the temperature dependence of the elastic constants, as discussed in detail above. It is of great interest to compare these constants with estimated values based on a point-charge calculation as given by Eq. (5). It is known that the crystal-field parameters describing the rare-earth energy levels are very close to parameters based on a point-charge calculation in the LnSb series.<sup>5</sup> Since the magnetoelastic coupling constants are the strain derivatives of the crystal-field parameters, they provide a sensitive test for the latter. They can decide whether or not a point-charge-calculation agreement is merely accidental. A comparison of the calculated values with the experimentally determined ones, all shown in Table II, immediately

shows a discrepancy of typically one order of magnitude, indicating that the agreement in the case of the crystal-field parameters was purely accidental.

Equation (5) indicates that the only variables changing across the series are the Stevens factor  $\alpha_J$ ,  $\langle r^2 \rangle$ , and the lattice constant  $2a$ . All these factors, with the exception of the exponent of  $a$ , are independent of the point-charge model. Therefore the variation of the  $g_i$  across the series should be well reproduced by estimates based on Eq. (5). This is indeed the case, as a comparison of the calculated and experimentally determined  $g_i$  indicates. The largest  $g_2$  occur for SmSb, the smallest for HoSb and ErSb, and the values for the other compounds lie in between. The combination of these coupling constants with the temperature-dependent function  $f$  gives the rich variety in  $c_{ij}(T)$  and structural  $T_a$ , as discussed above.

## V. SUMMARY

One of the main results of this study is the experimental determination of the magnetoelastic coupling constants and their interpretation for the LnSb series. The method of obtaining these parameters, from the temperature dependence of the elastic constants, is a new one. It should work whenever the crystal-field levels lie in the investigated temperature region. If one expresses the magnetoelastic energy in the usual form for a cubic material,  $E_m = b_2 \epsilon_{xy} \alpha_x \alpha_y + \dots$ , where  $\alpha_i$  are the direction cosines of the (sublattice) magnetization, the relation between  $b_i$  and  $g_i$  is  $b_2 = g_3 \times (c_0 N)^{1/2} J^2$ . For  $g_3 \sim 2 \text{ m}^\circ\text{K}$ ,  $b_2(T=0) \sim 10^6$  ergs/cm<sup>3</sup>, which is typical for rare-earth compounds.

From these magnetoelastic coupling constants we can understand, to a certain extent, the mechanisms of the low-temperature phase transition occurring in some of these compounds. The analysis gives for  $|g_2^2/g_3^2|$  the value of 3 for DySb, 0.2 for HoSb, and  $\ll 1$  for ErSb. The nature of the coupling constant  $g'$  is not known;  $k=0$  optical and acoustic phonons cannot contribute for the CsCl structure.<sup>11</sup> Direct and indirect electric-quadrupole and exchange interactions, as well as self-energy corrections, can contribute to  $g'$ .<sup>10</sup>

The nature of the phase transition is complicated. For DySb, HoSb, and ErSb, we found that the structural and magnetic transitions coincide. Different data suggest, furthermore, that the transitions in DySb and ErSb are of first order, while the one occurring in HoSb is possibly of second order. Finally, we showed that in ErSb a magnetic field cannot separate the structural and magnetic transitions, while in HoSb the evidence is not so clear. It is not yet clear whether all these properties can be explained with theoretical models employing dipolar and quadrupolar coupling.<sup>31</sup>

We have very few new data for the ordered re-

gion  $T < T_N$ . Domain-wall stress effects dominate the elastic behavior in this region. Magnetostriction data show complicated effects which probably have to do with the complicated magnetic structures encountered in these compounds.<sup>35</sup> These can best be interpreted with the tunneling model.<sup>29</sup>

Finally, it should be emphasized again that the new elastic effects due to crystal-field levels in these compounds are not confined to the LnSb series. Whenever one has crystal-field levels in the temperature region to be investigated, such effects should be observed.<sup>36</sup> In transition and actinide compounds this seems to be difficult to achieve. However, we have observed such effects in a number of other rare-earth compounds: TbP, TmTe, and Pr<sub>3</sub>S<sub>4</sub>.

*Note added in proof.* Calculations, analogous to Ref. 5 (1973), with  $Z = -1.3$ , relativistic  $\langle r^2 \rangle$  values and Sternheimer shielding factors,  $1 - \sigma_2$  ranging from 0.53 to 0.67 give an agreement with our experimental values within a factor of 2. We would like to thank Dr. R. J. Birgeneau for pointing these factors out to us.

#### ACKNOWLEDGMENTS

We are very much indebted to Dr. T. H. Henrie and Dr. M. M. Wong, U.S. Bureau of Mines, Reno, for supplying us with high-purity Pr metal.

#### APPENDIX: DERIVATION OF EQ. (9)

Consider the Hamiltonian in Eq. (8). Denote

$$\eta = g_2 \left( \frac{c_0}{N} \right)^{1/2} \epsilon_3 + g' \left( \frac{A}{N} \right)^{1/2} \langle O_2^0 \rangle.$$

Equation (3b) gives  $E(\Gamma_i) = E_{0i} + a_i \eta + b_i \eta^2$ . The free energy gives

$$F = \frac{1}{2} c_0 \epsilon_3^2 + \frac{1}{2} A \langle O_2^0 \rangle^2 - NkT \ln \sum_i e^{-\beta E_i}. \quad (\text{A1})$$

$\partial F / \partial \langle O_2^0 \rangle$  gives the order-parameter equation

$$A \langle O_2^0 \rangle = -g' \left( \frac{A}{N} \right)^{1/2} \frac{1}{Z} \sum_i e^{-\beta E_i} \frac{\partial E_i}{\partial \eta}.$$

Define the function

$$f_2 = \frac{d}{d\eta} \left( \frac{1}{Z} \sum_i e^{-\beta E_i} \frac{\partial E_i}{\partial \eta} \right) \\ = \frac{1}{Z} \sum_i e^{-\beta E_i} \frac{\partial^2 E_i}{\partial \eta^2} - \frac{\beta}{Z} \sum_i e^{-\beta E_i} \left( \frac{\partial E_i}{\partial \eta} \right)^2; \quad (\text{A2})$$

then

$$\frac{d \langle O_2^0 \rangle}{d \epsilon_3} = \frac{-g_2 g' (c_0 A)^{1/2} f_2 / N}{A + g'^2 f_2}.$$

The isothermal elastic constants are given by

$$c_T = \left( \frac{\partial^2 F}{\partial \epsilon_3^2} \right)_T. \quad (\text{A3})$$

Performing the differentiations using (A2) and  $d \langle O_2^0 \rangle / d \epsilon_3$  readily gives Eq. (9) of the text.

\*Work supported by the National Science Foundation.

†Work supported by the "Schweizer Nationalfonds."

<sup>1</sup>B. Lüthi, M. E. Mullen, and E. Bucher, Phys. Rev. Lett. **31**, 95 (1973).

<sup>2</sup>For a discussion of Schottky anomalies and Van Vleck susceptibilities, see, for example, C. Kittel, *Introduction to Solid State Physics*, 3rd ed. (Wiley, New York, 1966); B. R. Cooper, in *Magnetic Properties of Rare Earth Metals*, edited by R. J. Elliott (Plenum, New York 1972).

<sup>3</sup>H. R. Child, M. K. Wilkinson, J. W. Cable, W. C. Koehler, and E. O. Wollan, Phys. Rev. **131**, 922 (1963).

<sup>4</sup>F. Lévy, Phys. Kondens. Mater. **10**, 85 (1969).

<sup>5</sup>K. C. Turberfield, L. Passell, R. J. Birgeneau, and E. Bucher, J. Appl. Phys. **42**, 1746 (1971); R. J. Birgeneau, E. Bucher, L. Passell, and K. C. Turberfield, Phys. Rev. B **4**, 718 (1971); R. J. Birgeneau, E. Bucher, J. P. Maita, L. Passell, and K. C. Turberfield, *ibid.* **8**, 5345 (1973).

<sup>6</sup>M. T. Hutchings, in *Solid State Physics*, edited by F. Seitz and D. Turnbull (Academic, New York, 1964), Vol. 16, p. 227.

<sup>7</sup>K. R. Lea, M. J. M. Leask, and W. P. Wolf, J. Phys. Chem. Solids **23**, 1381 (1962).

<sup>8</sup>E. R. Callen and H. B. Callen, Phys. Rev. **129**, 578 (1963).

<sup>9</sup>M. Kataoka and J. Kanamori, J. Phys. Soc. Jap. **32**,

113 (1972).

<sup>10</sup>R. J. Elliott, R. T. Harley, W. Hayes, and S. R. P. Smith, Proc. R. Soc. A **328**, 217 (1972).

<sup>11</sup>P. Levy, J. Phys. C **6**, 3545 (1973).

<sup>12</sup>B. Lüthi, M. E. Mullen, K. Andres, E. Bucher, and J. P. Maita, Phys. Rev. B **8**, 2639 (1973).

<sup>13</sup>T. J. Moran, R. L. Thomas, P. M. Levy, and H. A. Chen, Phys. Rev. B **7**, 3238 (1973).

<sup>14</sup>R. L. Melcher and B. A. Scott, Phys. Rev. Lett. **28**, 607 (1972); J. R. Sandercock, S. B. Palmer, R. J. Elliott, W. Hayes, S. R. P. Smith, and A. P. Young, J. Phys. C **5**, 3126 (1972).

<sup>15</sup>Y. Kino, B. Lüthi, and M. E. Mullen, Solid State Commun. **12**, 275 (1973).

<sup>16</sup>R. M. Bozorth, H. J. Williams, and D. E. Walsh, Phys. Rev. **103**, 572 (1956).

<sup>17</sup>F. J. Morin and J. P. Maita, Phys. Rev. **129**, 1115 (1963).

<sup>18</sup>T. J. Moran and B. Lüthi, Phys. Rev. **187**, 710 (1969).

<sup>19</sup>E. Bucher, L. D. Longinotti, B. Lüthi, and M. E. Mullen, AIP Conf. Proc. **18**, 1298 (1973).

<sup>20</sup>D. T. Teaney, V. L. Moruzzi, and B. E. Argyle, J. Appl. Phys. **37**, 1122 (1966).

<sup>21</sup>H. Taub and S. J. Williamson, Solid State Commun. **13**, 1021 (1973).

<sup>22</sup>See, for example, R. Becker and W. Döring, *Ferro-magnetismus* (Springer, Berlin, 1939).

<sup>23</sup>B. Lüthi, T. J. Moran, and R. J. Pollina, J. Phys.

- Chem. Solids 31, 1741 (1970).
- <sup>24</sup>E. Bucher, R. J. Birgeneau, J. P. Maita, G. P. Felcher, and T. O. Brun, Phys. Rev. Lett. 28, 746 (1972).
- <sup>25</sup>G. Gorodetsky, Y. Kino, and B. Lüthi, in *Proceedings of the Conference on Phonon Scattering in Solids, Paris, 1972* (La Documentation Francaise, Paris, 1972), p. 333.
- <sup>26</sup>D. K. Ray and A. P. Young, J. Phys. C 6, 3353 (1973).
- <sup>27</sup>F. Hulliger and B. Natterer, Solid State Commun. 13, 221 (1973).
- <sup>28</sup>B. Lüthi and T. J. Moran, Phys. Rev. B 2, 1211 (1970).
- <sup>29</sup>K. W. H. Stevens and E. Pytte, Solid State Commun. 13, 101 (1973).
- <sup>30</sup>A measured point, not shown in Fig. 19, gives for  $H$  = 6.5 kOe and  $T = 3.42^\circ\text{K}$  an  $\alpha = 72 \times 10^{-5}^\circ\text{K}^{-1}$ .
- <sup>31</sup>See, for example, J. Sivardière and M. Blume, Phys. Rev. B 5, 1126 (1972); H. H. Chen and P. M. Levy, *ibid.* 7, 4267 (1973).
- <sup>32</sup>H. B. Huntington, in *Solid State Physics*, edited by F. Seitz and D. Turnbull (Academic, New York, 1964), Vol. 7, p. 213.
- <sup>33</sup>W. A. Harrison, *Pseudopotentials in the Theory of Metals* (Benjamin, New York, 1966), Chap. 6.
- <sup>34</sup>Tables used in G. A. Alers, in *Physical Acoustics IIB*, edited by W. P. Mason (Academic, New York, 1965).
- <sup>35</sup>H. R. Ott (unpublished).
- <sup>36</sup>Recently a similar effect has been observed for  $\text{TmVO}_4$ ; see R. L. Melcher, E. Pytte, and B. A. Scott, Phys. Rev. Lett. 31, 307 (1973). Their analysis relies on five-parameter fit.